

Article

## Structural insights into the mechanism of the radical SAM carbide synthase NifB, a key nitrogenase cofactor maturing enzyme

Ana Sosa Fajardo, Pierre Legrand, Lucía Payá-Tormo, Lydie Martin, MARIA TERESA PELLICER MARTINEZ, Carlos Echavarrri-Erasun, Xavier Vernède, Luis M. Rubio, and Yvain Nicolet

*J. Am. Chem. Soc.*, **Just Accepted Manuscript** • Publication Date (Web): 30 May 2020

Downloaded from [pubs.acs.org](https://pubs.acs.org) on May 30, 2020

### Just Accepted

“Just Accepted” manuscripts have been peer-reviewed and accepted for publication. They are posted online prior to technical editing, formatting for publication and author proofing. The American Chemical Society provides “Just Accepted” as a service to the research community to expedite the dissemination of scientific material as soon as possible after acceptance. “Just Accepted” manuscripts appear in full in PDF format accompanied by an HTML abstract. “Just Accepted” manuscripts have been fully peer reviewed, but should not be considered the official version of record. They are citable by the Digital Object Identifier (DOI®). “Just Accepted” is an optional service offered to authors. Therefore, the “Just Accepted” Web site may not include all articles that will be published in the journal. After a manuscript is technically edited and formatted, it will be removed from the “Just Accepted” Web site and published as an ASAP article. Note that technical editing may introduce minor changes to the manuscript text and/or graphics which could affect content, and all legal disclaimers and ethical guidelines that apply to the journal pertain. ACS cannot be held responsible for errors or consequences arising from the use of information contained in these “Just Accepted” manuscripts.

# Structural insights into the mechanism of the radical SAM carbide synthase NifB, a key nitrogenase cofactor maturing enzyme.

Ana Sosa Fajardo<sup>1,2</sup>, Pierre Legrand<sup>3</sup>, Lucía Payá-Tormo<sup>1,4</sup>, Lydie Martin<sup>2</sup>, Maria Teresa Pellicer Martínez<sup>1</sup>, Carlos Echavarri-Erasun<sup>1,4</sup>, Xavier Vernède<sup>2</sup>, Luis M. Rubio<sup>1,4\*</sup> and Yvain Nicolet<sup>2\*</sup>

<sup>1</sup>Centro de Biotecnología y Genómica de Plantas, Universidad Politécnica de Madrid, Instituto Nacional de Investigación y Tecnología Agraria y Alimentaria, Pozuelo de Alarcón, 28223 Madrid, Spain. <sup>2</sup>Univ. Grenoble Alpes, CEA, CNRS, IBS, Metalloproteins Unit, F-38000 Grenoble, France. <sup>3</sup>Synchrotron SOLEIL, L'Orme des Merisiers, Gif-sur-Yvette, France. <sup>4</sup>Departamento de Biotecnología-Biología Vegetal, Escuela Técnica Superior de Ingeniería Agronómica, Alimentaria y de Biosistemas, Universidad Politécnica de Madrid, 28040 Madrid, Spain.

**KEYWORDS** Radical SAM enzyme; Nitrogenase maturing enzyme; X-ray crystallography.

**ABSTRACT:** Nitrogenase is a key player in the global nitrogen cycle as it catalyzes the reduction of dinitrogen into ammonia. The active site of the nitrogenase MoFe protein corresponds to a [MoFe<sub>7</sub>S<sub>9</sub>C-(R)-homocitrate] species designated FeMo-cofactor, whose biosynthesis and insertion requires the action of over a dozen maturation proteins provided by the NIF (for Nitrogen Fixation) assembly machinery. Among them, the radical SAM protein NifB plays an essential role, concomitantly inserting a carbide ion and coupling two [Fe<sub>4</sub>S<sub>4</sub>] clusters to form a [Fe<sub>8</sub>S<sub>9</sub>C] precursor called NifB-co. Here we report on the X-ray structure of NifB from *Methanotrix thermoacetophila* at 1.95 Å resolution in a state pending the binding of one [Fe<sub>4</sub>S<sub>4</sub>] cluster substrate. The overall NifB architecture indicates that this enzyme has a single SAM binding site, which at this stage is occupied by cysteine residue 62. The structure reveals a unique ligand binding mode for the K1 cluster involving cysteine residues 29 and 128 in addition to histidine 42 and glutamate 65. The latter, together with cysteine 62, belongs to a loop inserted in the active site, likely protecting the already present [Fe<sub>4</sub>S<sub>4</sub>] clusters. These two residues regulate the sequence of events, controlling SAM dual reactivity and preventing unwanted radical-based chemistry before the K2 [Fe<sub>4</sub>S<sub>4</sub>] cluster substrate is loaded into the protein. The location of K1 cluster, too far away from the SAM binding site, supports a mechanism in which the K2 cluster is the site of methylation.

## INTRODUCTION

Nitrogenase catalyzes the reduction of atmospheric N<sub>2</sub> to 2 NH<sub>3</sub> at ambient temperature and normal pressure.<sup>1</sup> Its active site corresponds to a complex metallocluster whose archetype is the FeMo-co, a [MoFe<sub>7</sub>S<sub>9</sub>C-(R)-homocitrate] center that can be described as the combination of [MoFe<sub>3</sub>S<sub>3</sub>] and [Fe<sub>4</sub>S<sub>3</sub>] modules, connected via three μ<sub>2</sub>-sulfide and one μ<sub>6</sub>-carbide ions (Fig. 1a).<sup>2</sup> Variations of this center exists with molybdenum substituted by either iron or vanadium, defining three classes, Mo-, Fe- or V-nitrogenases.<sup>3</sup> The latter, in addition to the Mo to V substitution, also contains a carbonate ion replacing one of the μ<sub>2</sub>-sulfide ions.<sup>4</sup> Synthesis and insertion of FeMo-co in nitrogenase requires a set of accessory proteins named Nif proteins.<sup>5</sup> The key element of this assembly machinery is most probably the protein NifB, which performs the fusion of two [Fe<sub>4</sub>S<sub>4</sub>] centers and the concomitant production and insertion of one carbide ion and one additional sulfide ion. Whereas the chemistry at the heart of this reaction is still unknown, it has already been shown that NifB belongs to

the radical S-adenosyl-L-methionine (SAM) enzyme superfamily and uses radical-based chemistry to trigger the carbide production step.<sup>6,7</sup> The protein accommodates three [FeS] clusters: Two [Fe<sub>4</sub>S<sub>4</sub>] clusters designated as K1 and K2 and previously proposed to be modules of a larger cluster named K-cluster and a third [Fe<sub>4</sub>S<sub>4</sub>] cluster bound to the radical SAM-specific Cx<sub>3</sub>Cx<sub>2</sub>C conserved motif that we name RS-cluster.<sup>8,9</sup> The latter is dedicated to binding and reductive cleavage of SAM to produce a transient and highly reactive 5'-deoxyadenosyl radical (5'-dA•) species, which will trigger the radical-based reaction.<sup>10</sup> The two [Fe<sub>4</sub>S<sub>4</sub>] K1 and K2 clusters cannot be considered as cofactors as it is usually the case for FeS-cluster containing proteins, but rather as substrates for production of NifB-co, a [Fe<sub>8</sub>S<sub>9</sub>C] cluster precursor to FeMo-co (Scheme 1).<sup>11</sup> NifB-co is subsequently transferred to the scaffold protein NifEN<sup>12,13</sup> where it is further modified, including Mo insertion and R-homocitrate binding.<sup>5</sup> Radioactive isotopic labelling experiments demonstrated that the carbide ion originates from the methyl group of one SAM molecule.<sup>7</sup> Site-directed mutagenesis experiments combined with

spectroscopic characterization support a direct attack of one sulfide ion from the K2 cluster on the methyl following an  $S_N2$  mechanism.<sup>14</sup> A second SAM molecule is subsequently used to produce 5'-dA• and to abstract one hydrogen atom from the above-mentioned methyl fragment, the remaining hydrogens are most likely removed through deprotonations.<sup>7</sup> Combining site-directed mutagenesis and electron paramagnetic resonance spectroscopy, the K1 cluster has been proposed to bind to three cysteine residues (C<sup>29</sup>, C<sup>62</sup> and C<sup>128</sup>, equivalent to C<sup>30</sup>, C<sup>63</sup> and C<sup>129</sup> in *Methanosarcina acetivorans* NifB numbering) and a histidine, very recently identified as H<sup>42</sup> (H<sup>43</sup> in *M. acetivorans*)<sup>9,14,15</sup> The K2 cluster is also proposed to bind to two or three cysteines (C<sup>273</sup> and C<sup>276</sup> equivalent to C<sup>274</sup> and C<sup>277</sup>, in addition to C<sup>264</sup> in *M. acetivorans*) and presumably another unidentified ligand.<sup>9,14</sup> It was reported that the redox status of the three different clusters might trigger methyl transfer and SAM cleavage.<sup>14,16</sup> K1 and K2 clusters would provide eight out of the nine sulfide ions of NifB-co and a recent study has indicated that the ninth sulfide originates *in vitro* from the reduction of a sulfite ion involving an unknown mechanism.<sup>17</sup>

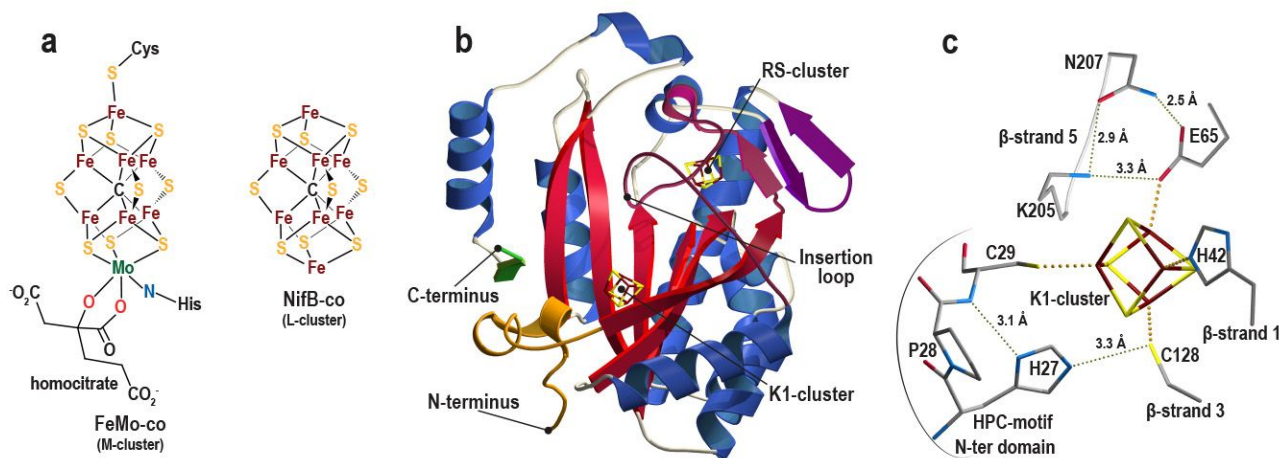
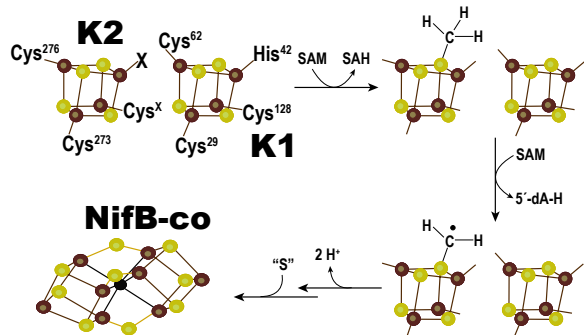


**Figure 1.** a: Structure of the FeMo-co and proposed model of the NifB-co (left and right, respectively). b: overall structure of NifB. The RS-core is depicted in red ( $\beta$ -strands) and blue ( $\alpha$ -helices). The N- and C-terminal stretches are depicted in orange and green, respectively. The insertion loop and the additional  $\beta$ -sheet are represented in purple. The K1 and RS-clusters are depicted in ball-and-stick. c: Stick representation of the K1-cluster environment.

The crystal structure corresponds to a  $(\beta\alpha)_6$  three-quarter barrel typical of radical SAM enzymes, sandwiched by short N- and C-terminal stretches (in orange and green, respectively in Figure 1b). Residues 1-19 and 272-299 are missing in the structure probably due to disorder.

**Scheme 1.** Reaction catalyzed by NifB. Only the main identified steps are presented. The residue numbering corresponds to that of the NifB protein from *Methanotrix thermoacetophila*. S, Fe and C atoms are represented as yellow, brown and black spheres, respectively.

Here we report the first crystal structure of NifB in complex with the RS-cluster cofactor and one of its substrates, the K1-cluster. A specific loop bridges the RS- and K1-clusters and contains residues involved in preventing unproductive SAM cleavage. This structure also suggests large structural motions during turnover to afford K1 and K2 cluster fusion and NifB-co synthesis. This crystal structure likely corresponds to one of the early states during the highly complex carbide insertion and FeS cluster fusion processes catalyzed by NifB.

## RESULTS AND DISCUSSION

**X-ray crystal structure of NifB.** The lack of further structural details has impaired a better understanding of the mechanism of NifB-co synthesis. To determine its tridimensional structure, we sought to obtain crystals of 8 NifB orthologues lacking the C-terminal NifX-like domain often observed in NifB proteins. The NifX-like domain is not essential for NifB-co synthesis<sup>18,19</sup>. Brownish thin plate crystals were obtained for NifB from the archaeon *Methanotrix thermoacetophila* PT (GenBank ID: ABK14214.1) (See Methods). The crystal structure was solved by a combination of single wavelength anomalous dispersion (SAD) phasing and molecular replacement and was refined to 1.95 Å resolution (see Supplementary Methods and Table S1; PDB ID: 6Y1X). Albeit crystals contain two molecules per asymmetric unit, analysis of the intermolecular interaction<sup>20</sup> confirms the protein is a monomer, in agreement with the previous characterization of other archaeal NifB proteins.<sup>9,18,19</sup>

Structural comparison with all available structures from the Protein Data Bank indicates that the radical SAM core domain, which corresponds to residues 39-266 is very similar to that of the radical SAM pyruvate formate-lyase activating enzyme (Figure S1).<sup>21</sup> Indeed, despite only

21% amino acid sequence identity, the two structures superimpose with a root mean square deviation of 2.8 Å over 204 aligned C $\alpha$  atoms. The main noteworthy differences lie in the length of the loops that connect the Cx<sub>3</sub>Cx<sub>2</sub>C motif and helix  $\alpha_1$ , helices  $\alpha_{4A}$  and  $\alpha_4$  and strand  $\beta_6$  and helix  $\alpha_6$  (Figure 1b and Figures S1 and S2.).

The Fe content, UV-visible spectrum, and NifB-co synthesis activity of the wild type variant of as purified *Mt*NifB is consistent with partial [Fe<sub>4</sub>S<sub>4</sub>] cluster occupancy or with a mixture of species. However, the enzyme was active to produce NifB-co (Figures S3–S5 Tables S2–S4) when reductant and SAM were provided. Aiming at obtaining a crystal structure containing three [Fe<sub>4</sub>S<sub>4</sub>] clusters, the latters were chemically reconstituted (see Supplementary methods), leading to NifB preparations containing 12–14 iron atoms per monomer. However, the as-solved NifB structure harbors only the RS- and K1 clusters (Figures S6 and S7). The former corresponds to the cofactor responsible for SAM binding and cleavage. It is bound to cysteine residues 49, 53 and 56 defining the Cx<sub>3</sub>Cx<sub>2</sub>C motif. Despite incubating the protein with excess of SAM during the crystallization trials, the unique Fe site of the RS-cluster, which naturally binds SAM, is bound to the cysteine residue 62, which belongs to the longer loop observed between the Cx<sub>3</sub>Cx<sub>2</sub>C motif and helix  $\alpha_1$  (Figures S2 and S8). This cysteine residue is strictly conserved in NifB proteins and has been previously proposed to provide a ligand to the K1 cluster.<sup>14</sup> Indeed, when searching for residues that could be ligands of the different clusters, series of triple cysteine to alanine variants were produced (C<sup>49</sup>, C<sup>52</sup> and C<sup>56</sup> for the RS-cluster; C<sup>29</sup>, C<sup>62</sup> and C<sup>128</sup> for the K1 cluster; C<sup>273</sup> and C<sup>276</sup> and an additional cysteine residue not conserved in *M. thermoacetophila* for the K2 cluster). They all led to NifB proteins that are unable to produce NifB-co, highlighting the essential role of these ligands.<sup>9,14</sup> However, these experiments corresponded to triple cysteine to alanine conversions that are expected to be more drastic than single residue modifications. The C<sup>62</sup>S substitution leads to a strong decrease in the NifB enzyme activity (Figure 2) even though its Fe content is only slightly affected and its UV-vis spectrum unaltered (Figures S3 and S4 and Table S2). This suggests C<sup>62</sup> may not be involved in K1-cluster binding as previously proposed, at least at the early reaction stages. Furthermore, despite the unique Fe site is bound to C<sup>62</sup>, the remaining SAM-binding motifs are present and structurally localized in a pre-organized site to house SAM once C<sup>62</sup> would come off (Figure S9). No obvious additional SAM binding site was detected, suggesting the two SAM molecules would bind to the RS-cluster as previously observed in other radical SAM methyl transferases such as RlmN.<sup>22</sup> It is noteworthy that in the latter enzymes, a cysteine residue is in a flexible loop and is involved in methyl transfer. However, such a role for cysteine 62 can be excluded in NifB, as the C<sup>62</sup> to alanine mutant functions in methyl transfer.<sup>14</sup> This deduction is further supported by the fact that no detection of a methylated cysteine residue has yet been reported in NifB.<sup>14</sup> Conversely, the C<sup>62</sup>S variant exhibits a five-fold increase in the 5'-dA/SAH ratio when compared to the wild-type enzyme (Table 1), suggesting this residue is involved in the control of SAM-binding/cleavage in order to orchestrate an efficient methyl transfer and H-atom

abstraction. To the best of our knowledge, this would be the first example of a protein residue competing with SAM for fixation to the RS-cluster for regulation purposes.

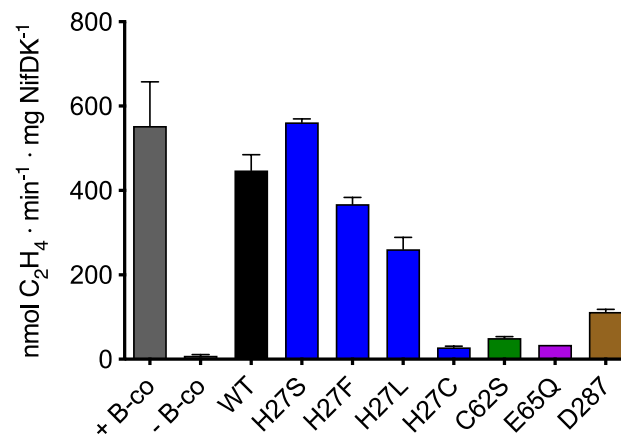


**Figure 2.** Activity of purified NifB site-directed variants. The ability of NifB variants to support NifB-dependent *in vitro* FeMo-co synthesis is estimated by the activities of cofactor-reconstituted NifDK. Reactions contained 2 nmol of NifB and 0.06 nmol NifDK in a final volume of 100  $\mu$ l. Reactions lacking NifB but containing 0.255 nmol of NifB-co were used as positive controls and yielded  $552 \pm 104$  nmol C<sub>2</sub>H<sub>4</sub>·min<sup>-1</sup>·mg NifDK<sup>-1</sup>. Data are the average  $\pm$  SD of at least two independent determinations with two replicates each.

**Table 1. SAH and 5'-dA production by NifB wild type (WT) and site-directed variants.**

Variant	SAH	5'-dA	5'-dA/SAH
WT	0.43 $\pm$ 0.02	0.88 $\pm$ 0.09	2.0
H27S	0.10 $\pm$ 0.02	0.21 $\pm$ 0.04	2.1
H27F	0.07 $\pm$ 0.01	0.16 $\pm$ 0.02	2.3
H27L	0.04 $\pm$ 0.01	0.11 $\pm$ 0.01	2.7
H27C	0.01 $\pm$ 0.01	0.04 $\pm$ 0.007	4.0
C62S	0.27 $\pm$ 0.03	2.71 $\pm$ 0.76	10.0
E65Q	0.22 $\pm$ 0.004	1.21 $\pm$ 0.06	5.5
D287Stop	0.09 $\pm$ 0.01	0.11 $\pm$ 0.01	1.2

Reactions contain 13 nmol NifB in 650  $\mu$ l. SAH and 5'-dA produced are indicated as nmol product per nmol NifB per hour  $\pm$  SD (Data are the average of at least two independent determinations with two replicates each).

The K1-cluster, which corresponds to one of the substrates of the enzyme is bound to the strictly conserved residues cysteine 29 and 128 as was previously proposed,<sup>9,14</sup> histidine 42 and, unexpectedly, to glutamate 65 (Figure 1c). To the best of our knowledge,<sup>23</sup> this represents the first case of mixed coordination of a [Fe<sub>4</sub>S<sub>4</sub>] cluster that involves two cysteines, one histidine and one glutamate. Unusual FeS-cluster non-cysteinyll residue ligands are also observed in lipoic acid synthase and biotin synthase, two radical SAM enzymes that use FeS clusters as substrates.<sup>24,25</sup> In the former, a serine ligand is exchanged upon substrate binding to allow C-S bond formation. In the latter, the additional arginine

residue coordinates both one iron and one sulfide ions of the  $[\text{Fe}_5\text{S}_2]$  cluster, further modulating its properties and likely facilitating sulfide transfer during biotin synthesis.<sup>26</sup> In NifB, such peculiar ligand coordination may also be related to the substrate status of this cluster that has to be fused to K2 when forming NifB-co. C<sup>29</sup> belongs to the small N-terminal stretch specific to NifB, where it falls in a conserved HPC-motif. The histidine residue H<sup>27</sup> from this HPC-motif does not bind the K1 cluster but is sandwiched between the two cysteine ligands. Despite its strict conservation in NifB, substitution of H<sup>27</sup> does not significantly affect the activity of the protein (Figure 2). Its replacement by a cysteine residue, however, does induce a drop in the activity, most probably due to the presence of a thiol group, which may affect the integrity of the K1-cluster, perhaps by forming a disulfide bond with either C<sup>29</sup> or C<sup>128</sup>, thus preventing K1-cluster binding (Figure 1c and Tables S2 and S4). Thus, despite being conserved, H<sup>27</sup> does not appear to play an essential role in the NifB activity. Residues H<sup>42</sup> and C<sup>128</sup> belong to the radical SAM core domain where they are located in strands  $\beta_1$  and  $\beta_3$ , respectively. This coordination anchors the K1-cluster at about 12 Å away from the RS-center. Such separation agrees with the previous observation that the initial methyl transfer from SAM involves the K2-module and not K1<sup>14</sup> because the latter is too far away and is positioned in a rigid structure that likely precludes movement. However, during NifB-co synthesis, it has been shown that the interaction observed between H<sup>42</sup> and K1 is lost upon NifB-co formation,<sup>14</sup> supporting ligand exchange and presumably displacement of the K1-center upon cluster fusion. A very recent study proposed that H<sup>42</sup> would have a dual role in coordinating K1 cluster and acting as a base for the subsequent deprotonations of the methylene group upon carbide synthesis.<sup>15</sup> Like residue C<sup>62</sup>, E<sup>65</sup> is strictly conserved within NifB proteins and belongs to the long loop between the  $\text{C}_x\text{C}_x\text{C}_2\text{C}$  motif and helix  $\alpha_1$ . Its length, unique in all the radical SAM protein structures known to date, allows the tip to reach the active site with residues C<sup>62</sup>VNE<sup>65</sup> sitting into the cavity defined by the  $\beta$ -strands and corresponding to where substrate usually binds in these proteins (Figures 3a and S8). While bound to K1, E<sup>65</sup> faces and interacts with two strictly conserved residues K<sup>205</sup> and N<sup>207</sup> from  $\beta$ -strand 5 (Figure 1c). Like the C<sup>62</sup>S variant, the E<sup>65</sup>Q substituted protein displays a significant drop in the NifB activity (Figure 2) and an increase in the 5'-dA/SAH ratio (Table 1), without abolishing the activity. This is in striking contrast with the previously reported substitution of residue H<sup>42</sup> leading to inactive protein.<sup>15</sup> Thus, while H<sup>42</sup> is key for the reaction, the loop containing both C<sup>62</sup> and E<sup>65</sup> would rather act as a controller to avoid unwanted decoupling between methyl transfer and SAM cleavage by most likely regulating SAM access to the active site.

This C<sup>62</sup>VNE<sup>65</sup> tip spans over the cavity such that C<sup>62</sup> and E<sup>65</sup> are ideally oriented to bind the RS- and K1-clusters, respectively. However, close inspection of the overall NifB structure indicates that C<sup>62</sup> is the only residue that falls into the disallowed region of the Ramachandran plot<sup>27</sup> outlining conformational strain upon binding to the RS-cluster. Strikingly, both molecules in the asymmetric unit exhibit the exact same conformation for this loop, supporting the conclusion this state is energetically

favorable, despite the presence of excess of SAM in the crystallization conditions. This observation is also in agreement with the previous observation that despite incubation with SAM in solution, no interaction between SAM and the RS-cluster can be detected,<sup>9</sup> further suggesting that SAM binding might depend on whether other substrates, namely the K1 and K2 clusters, are already present. However, such strain around C<sup>62</sup> suggests that a slight conformational change would trigger the release of the unique Fe site in the RS-cluster and consequently would allow SAM binding for the reaction to proceed. As was shown previously, reduction of the clusters is required to trigger methyl transfer to K2 and possibly linked to SAM binding.<sup>14</sup> RS-cluster reduction or possibly K1 reduction, could thus precede SAM binding and provide the necessary signal to induce the motion of the C<sup>62</sup>-E<sup>65</sup> loop<sup>16</sup>. *In vivo*, such reduction might be performed by a ferredoxin such as the one encoded by the *fdxN* gene, located downstream NifB in the NIF gene cluster of *Azotobacter vinelandii*, as previously proposed.<sup>5</sup>

**Absence of the K2 cluster.** Despite numerous attempts to keep the K2-cluster bound to NifB, crystals with K2 present were not obtained. The last residue for which interpretable electron density is observed corresponds to R<sup>271</sup>, which follows the last helix of the RS-core domain and is located in a seventh  $\beta$ -strand. The two cysteine residues C<sup>273</sup> and C<sup>276</sup> both previously identified as ligands of the K2-cluster are next to this last residue, suggesting where K2 should sit at the surface of the protein, solvent exposed and overhanging the active site cleft, which could explain why K2 is so unstable and may be lost during the time course of the crystallization process. The R<sup>271</sup> residue is equivalent to the last residue in Pfl-ae, the closest RS-enzyme structure to NifB. Furthermore, the second closest structure corresponds to SuiB, a RS-enzyme involved in the post-translational modification of ribosomally synthesized peptides that contains additional clusters in a SPASM domain at its C-terminus stretch.<sup>28</sup> In SuiB, a  $\beta$ -strand connects the RS-core and the SPASM domains. The first cysteine residue that binds one of the  $[\text{Fe}_4\text{S}_4]$  clusters of the SPASM domain is located one residue after C<sup>273</sup> in NifB when comparing their amino acid sequence alignments, further indicating where K2 might be located (Figure 3b). Other than C<sup>273</sup> and C<sup>276</sup>, there are no obvious conserved residue that are candidates to bind the K2-cluster. The only potential residue located nearby corresponds to cysteine C<sup>35</sup>. However, in addition to its non-conservation among the known NifB sequences, such binding would lock the K2-cluster farther than 15 Å away from the RS-cluster, impairing both direct methyl transfer from SAM and subsequent H-atom abstraction. The crystal structure instead suggests the K2-cluster is bound exclusively to the C-terminal stretch through C<sup>273</sup> and C<sup>276</sup> and possibly the strictly conserved residue D<sup>279</sup>. Such binding mode would allow the K2-cluster to oscillate from a resting position exposed to solvent to another position located closer to the RS-cluster to enable direct methyl transfer and subsequent cluster fusion. In this model, the C<sup>62</sup>-E<sup>65</sup> residue containing loop must leave the active site to permit both SAM binding and K2-cluster access.

1  
2  
3  
4  
5  
6  
7  
8  
9  
10  
11  
12  
13  
14  
15  
16  
17  
18  
19  
20  
21  
22  
23  
24  
25  
26  
27  
28  
29  
30  
31  
32  
33  
34  
35  
36  
37  
38  
39  
40  
41  
42  
43  
44  
45  
46  
47  
48  
49  
50  
51  
52  
53  
54  
55  
56  
57  
58  
59  
60

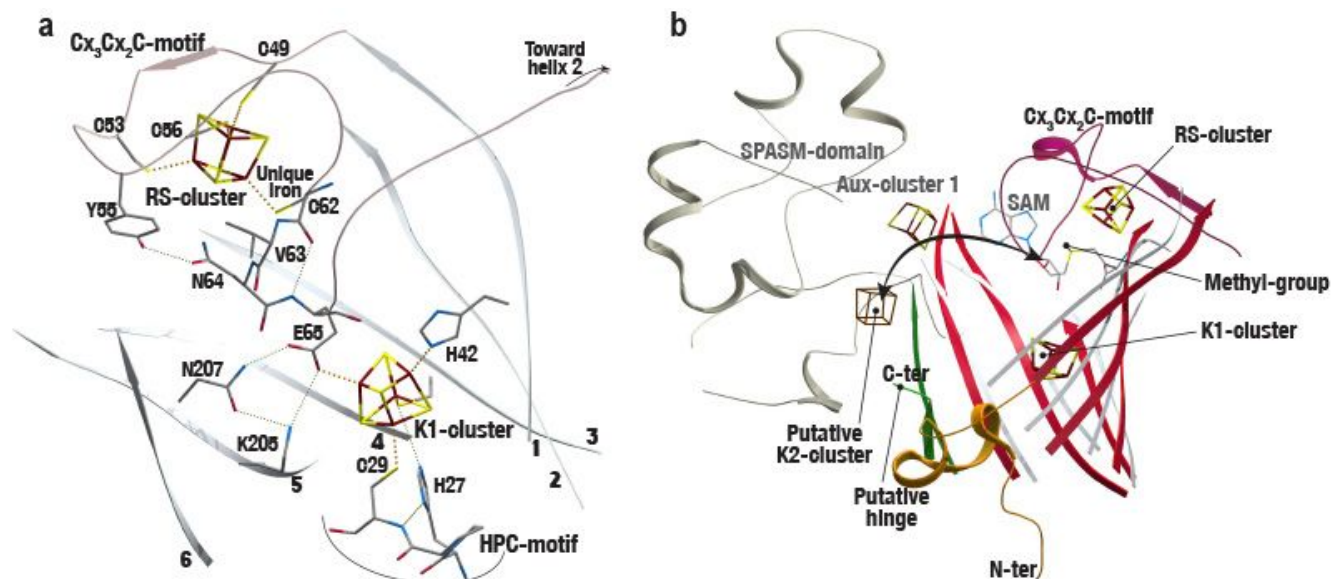


**Figure 3. a:** View of the loop connecting the RS- and K1-clusters. Only the amino acids at the tip ( $C^{62}VNE^{65}$ ) are depicted in sticks. The rest of the loop is depicted as a grey coil. The surrounding  $\beta$ -strands are depicted in grey and their relative number indicated in bold. **b:** Superposition of the radical SAM cores of NifB and SuiB (PDB ID: 5V1S). The following  $\beta$ -strand in both structures are represented in green. The SuiB SPASM-domain and first auxiliary cluster are also represented in grey. The deduced location of the K2-cluster in NifB is drawn as a brown cubane.

Adjacent to the C-terminal  $Cx_2Cx_2Dx_2G$ -motif, NifB primary structures usually include a lysine-rich region sometimes followed by an additional NifX-like domain proposed to house the NifB-co prior to its transfer to NifEN (Figure S2).<sup>29</sup> Lysine-rich regions are often involved in protein-protein, protein-nucleic acid or protein-cofactor interactions.<sup>30,31</sup> In NifB, its vicinity to the K2-cluster binding site suggested either this region being involved in the interaction with NifU for a facile  $[Fe_4S_4]$ -cluster insertion or in the interaction with NifEN for subsequent NifB-co transfer. However, removal of the thirteen last residues leads to a protein with altered activity *in vitro* (Figure 2 and Table 1), outlining such modification, while not being deleterious, should affect the nearby K2-cluster stability and impacts both methyl transfer and SAM cleavage.

**Proposed structural mechanism of NifB for NifB-co biosynthesis.** The NifB crystal structure combined with site-directed mutagenesis supports the early steps in the following sequential events during NifB-co synthesis (Figure 4). Starting with NifB containing only the RS-cluster (1 in Figure 4), the K1 cluster may be first delivered by NifU, a scaffold protein in which  $[Fe_4S_4]$  clusters are assembled to be later delivered to many Nif client proteins.<sup>5</sup> In fact, NifU has been shown to be the major provider of  $[Fe_4S_4]$  clusters for NifB-co biosynthesis.<sup>32</sup> The  $C^{62}$ - $E^{65}$  residue-containing loop would stabilize this state by binding to both the RS- and K1-clusters as observed in our reported the crystal structure (2 in Figure 4). Upon K2-cluster insertion (3) and presumably K1-cluster reduction<sup>16</sup> (4),  $E^{65}$  would come off K1-cluster entailing  $C^{62}$  to pull away from the RS-cluster thereby allowing SAM to bind and K2-cluster to move forward to capture the methyl group (5) on one of the sulfide ions.<sup>14</sup> Subsequently, a second SAM molecule would replace the produced SAH (6) and homolytic SAM cleavage would proceed to catalyze the radical-based hydrogen-atom abstraction

from the methyl group (7). Two successive deprotonations recently proposed to be catalyzed by the histidine residue 42<sup>15</sup> would follow concomitantly with the beginning of K1-K2 cluster fusion. Ligands exchanges for both K1 and K2 might be assisted by the  $C^{62}$  and  $E^{65}$  residues to perform this fusion and form a  $[Fe_8S_8C]$ -cluster precursor of the NifB-co precursor (8). Production and insertion of the 9<sup>th</sup> sulfur atom would take place at the end of the reaction (9) as suggested by the characterization or the  $[Fe_8S_8C]$ -cluster precursor that lacks it.<sup>33</sup> It has been reported that sulfite ion can be the sulfur source *in vitro*,<sup>17</sup> yet no clear mechanism for sulfite reduction to sulfide can be deduced from the NifB structure. One cannot exclude that a different sulfur source occurs *in vivo*. This succession of events and the high complexity of the reaction most likely requires large conformational changes and further structural characterizations are needed to understand this  $[Fe_4S_4]$  cluster fusion. In addition, interaction with the Nif-partners likely plays a fundamental role *in vivo*, notably with electron-carriers such as FdxN to carry out all the required reductions over this complex process.<sup>34</sup> Our crystal structure paves the way to understand at the molecular level how NifB catalyzes such a difficult reaction in biology. Structural features reported here cast some doubts about the former definition for K1- and K2-clusters as being modules of a larger cluster<sup>14</sup> and instead suggest they are independent entities sequentially loaded into the protein matrix. Furthermore, they must be considered as substrates and not cofactors of the enzyme. The identified insertion loop tightly controls SAM binding and suggests how a protein of less than 300 amino acids can perform such a multistep reaction, which includes a methyl transfer, a radical-based H-atom abstraction, several deprotonations and extensive  $[Fe_4S_4]$  center ligand exchanges to fuse two clusters into a unique  $[Fe_8S_9C]$ .

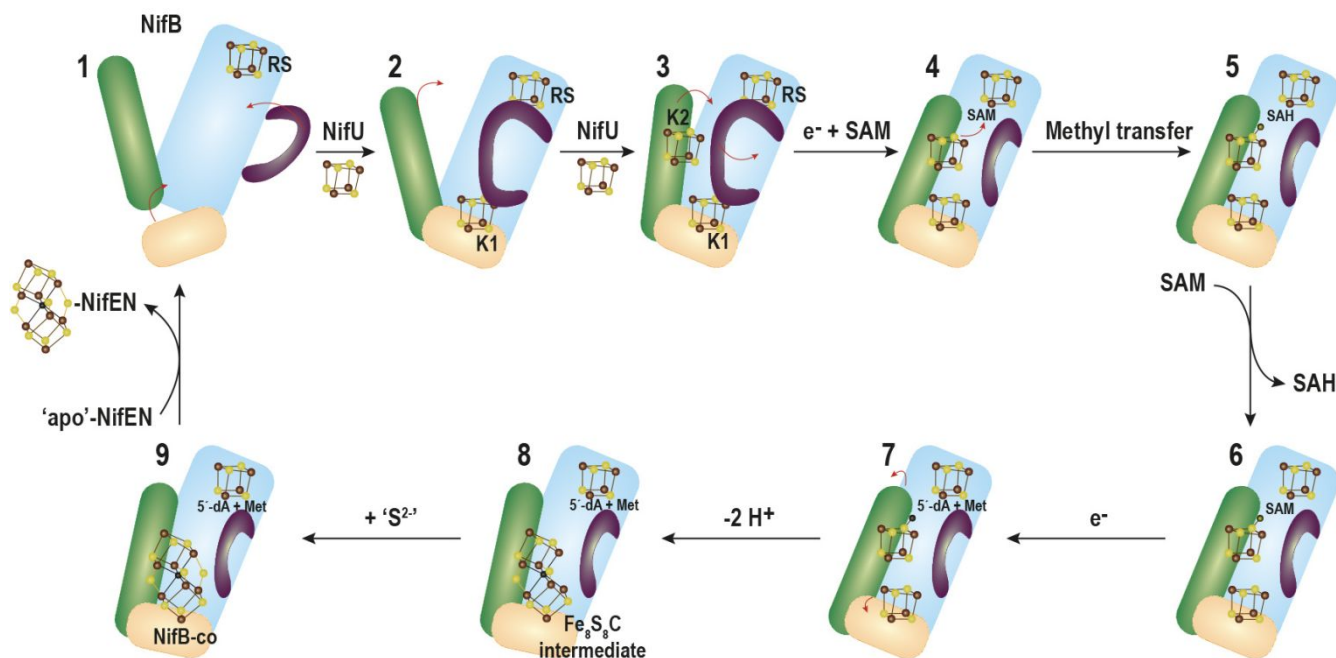


**Figure 4.** The NifB structure is schematized as a blue rectangle corresponding to the radical SAM core structure, flanked by N- and C-terminus stretches (orange and green rectangles, respectively). The C<sup>62</sup>-containing loop is depicted in purple. The proposed domain movements are indicated by red arrows. The FeS cluster and carbon atoms are depicted as ball-and-stick (iron, sulfur and carbon in brown, yellow and black spheres, respectively). The presented crystal structure corresponds to species **2**.

## ASSOCIATED CONTENT

### Supporting Information

The experimental material and methods, X-ray data collection and refinement statistics, supplementary figures and tables.

The Supporting Information is available free of charge on the ACS Publications website.

## AUTHOR INFORMATION

### Corresponding Author

\* Correspondence and request for materials should be addressed to [lm.rubio@upm.es](mailto:lm.rubio@upm.es) or [yvain.nicolet@ibs.fr](mailto:yvain.nicolet@ibs.fr).

### Author Contributions

## ACKNOWLEDGMENT

This work was supported by FEDER / Ministerio de Ciencia, Innovación y Universidades – Agencia Estatal de Investigación / Proyecto 2017-88475-R to L.M.R and by the French National Research Agency in the framework of the Investissements d’Avenir program (ANR-15-IDEX-02), through the funding of the "Origin of Life" project of the Univ. Grenoble-Alpes. L. P.-T. is recipient of the FPU16/02284 from Ministerio de Ciencia, Innovación y Universidades. This work used the platforms of the Grenoble Instruct-ERIC center (ISBG; UMS 3518 CNRS-CEA-UGA-EMBL) within the Grenoble Partnership for Structural Biology (PSB), supported by FRISBI (ANR-10-INBS-05-02) and GRAL, financed within the University Grenoble Alpes graduate school (Ecoles Universitaires de Recherche) CBH-EUR-GS (ANR-17-EURE-0003).

## REFERENCES

- (1) Hoffman, B. M.; Lukoyanov, D.; Yang, Z.-Y.; Dean, D.

R.; Seefeldt, L. C. Mechanism of Nitrogen Fixation by Nitrogenase: The next Stage. *Chem. Rev.* **2014**, *114* (8), 4041–4062.

(2) Spatzal, T.; Aksoyoglu, M.; Zhang, L.; Andrade, S. L. A.; Schleicher, E.; Weber, S.; Rees, D. C.; Einsle, O. Evidence for Interstitial Carbon in Nitrogenase FeMo Cofactor. *Science* **2011**, *334* (6058), 940.

(3) Bishop, P.; Joerger, R. Genetics and Molecular Biology of Alternative Nitrogen-Fixation Systems. *Annu. Rev. Plant Physiol. Plant Mol. Biol.* **1990**, *41*, 109–125.

(4) Harris, D. F.; Lukoyanov, D. A.; Kallas, H.; Trncik, C.; Yang, Z.-Y.; Compton, P.; Kelleher, N.; Einsle, O.; Dean, D. R.; Hoffman, B. M.; Seefeldt, L. C. Mo-, V-, and Fe-Nitrogenases Use a Universal Eight-Electron Reductive-Elimination Mechanism To Achieve N<sub>2</sub> Reduction. *Biochemistry* **2019**, *58* (30), 3293–3301.

(5) Buren, S.; Jimenez-Vicente, E.; Echavarri-Erasun, C.; Rubio, L. M. Biosynthesis of Nitrogenase Cofactors. *Chem. Rev.* **2020**. <https://doi.org/10.1021/acs.chemrev.9b00489>.

(6) Curatti, L.; Ludden, P. W.; Rubio, L. M. NifB-Dependent in Vitro Synthesis of the Iron-Molybdenum Cofactor of Nitrogenase. *Proc. Natl. Acad. Sci. U. S. A.* **2006**, *103* (14), 5297–5301.

(7) Wiig, J. A.; Hu, Y.; Chung Lee, C.; Ribbe, M. W. Radical SAM-Dependent Carbon Insertion into the Nitrogenase M-Cluster. *Science* **2012**, *337* (6102), 1672–1675.

(8) Wiig, J. A.; Hu, Y.; Ribbe, M. W. NifEN-B Complex of *Azotobacter vinelandii* Is Fully Functional in Nitrogenase FeMo Cofactor Assembly. *Proc. Natl. Acad. Sci. U. S. A.* **2011**, *108* (21), 8623–8627.

(9) Wilcoxon, J.; Arragain, S.; Scandurra, A. A.; Jimenez-Vicente, E.; Echavarri-Erasun, C.; Pollmann, S.; Britt, R. D.; Rubio, L. M. Electron Paramagnetic Resonance Characterization of Three Iron-Sulfur Clusters Present in the Nitrogenase Cofactor Maturase NifB from *Methanocaldococcus infernus*. *J. Am. Chem. Soc.* **2016**, *138* (24), 7468–7471.

(10) Broderick, J. B.; Duffus, B. R.; Duschene, K. S.; Shepard, E. M. Radical S-Adenosylmethionine Enzymes. *Chem.*

Rev. **2014**, *114* (8), 4229–4317.

(11) Guo, Y.; Echavarri-Erasun, C.; Demuez, M.; Jimenez-Vicente, E.; Bominaar, E. L.; Rubio, L. M. The Nitrogenase FeMo-Cofactor Precursor Formed by NifB Protein: A Diamagnetic Cluster Containing Eight Iron Atoms. *Angew. Chem. Int. Ed Engl.* **2016**, *55* (41), 12764–12767.

(12) Allen, R. M.; Chatterjee, R.; Ludden, P. W.; Shah, V. K. Incorporation of Iron and Sulfur from NifB Cofactor into the Iron-Molybdenum Cofactor of Dinitrogenase. *J. Biol. Chem.* **1995**, *270* (45), 26890–26896.

(13) Kaiser, J. T.; Hu, Y.; Wiig, J. A.; Rees, D. C.; Ribbe, M. W. Structure of Precursor-Bound NifEN: A Nitrogenase FeMo Cofactor Maturase/Insertase. *Science* **2011**, *331* (6013), 91–94.

(14) Rettberg, L. A.; Wilcoxon, J.; Lee, C. C.; Stiebritz, M. T.; Tanifuji, K.; Britt, R. D.; Hu, Y. Probing the Coordination and Function of Fe<sub>4</sub>S<sub>4</sub> Modules in Nitrogenase Assembly Protein NifB. *Nat. Commun.* **2018**, *9* (1), 2824.

(15) Rettberg, L. A.; Wilcoxon, J.; Jasniewski, A. J.; Lee, C. C.; Tanifuji, K.; Hu, Y.; Britt, R. D.; Ribbe, M. W. Identity and Function of an Essential Nitrogen Ligand of the Nitrogenase Cofactor Biosynthesis Protein NifB. *Nat. Commun.* **2020**, *11* (1), 1757.

(16) Wiig, J. A.; Hu, Y.; Ribbe, M. W. Refining the Pathway of Carbide Insertion into the Nitrogenase M-Cluster. *Nat. Commun.* **2015**, *6*, 8034.

(17) Tanifuji, K.; Lee, C. C.; Sickerman, N. S.; Tatsumi, K.; Ohki, Y.; Hu, Y.; Ribbe, M. W. Tracing the “ninth Sulfur” of the Nitrogenase Cofactor via a Semi-Synthetic Approach. *Nat. Chem.* **2018**, *10* (5), 568–572.

(18) Fay, A. W.; Wiig, J. A.; Lee, C. C.; Hu, Y. Identification and Characterization of Functional Homologs of Nitrogenase Cofactor Biosynthesis Protein NifB from Methanogens. *Proc. Natl. Acad. Sci. U. S. A.* **2015**, *112* (48), 14829–14833.

(19) Arragain, S.; Jimenez-Vicente, E.; Scandurra, A. A.; Buren, S.; Rubio, L. M.; Echavarri-Erasun, C. Diversity and Functional Analysis of the FeMo-Cofactor Maturase NifB. *Front. Plant Sci.* **2017**, *8*, 1947.

(20) Krissinel, E.; Henrick, K. Inference of Macromolecular Assemblies from Crystalline State. *J. Mol. Biol.* **2007**, *372* (3), 774–797.

(21) Vey, J. L.; Yang, J.; Li, M.; Broderick, W. E.; Broderick, J. B.; Drennan, C. L. Structural Basis for Glycyl Radical Formation by Pyruvate Formate-Lyase Activating Enzyme. *Proc. Natl. Acad. Sci. U. S. A.* **2008**, *105* (42), 16137–16141.

(22) Boal, A. K.; Grove, T. L.; McLaughlin, M. I.; Yennawar, N. H.; Booker, S. J.; Rosenzweig, A. C. Structural Basis for Methyl Transfer by a Radical SAM Enzyme. *Science* **2011**, *332* (6033), 1089–1092.

(23) Volbeda, A.; Martinez, M. T. P.; Crack, J. C.; Amara, P.; Gigarel, O.; Munnoch, J. T.; Hutchings, M. I.; Darnault, C.; Le Brun, N. E.; Fontecilla-Camps, J. C. Crystal Structure of the Transcription Regulator RsrR Reveals a [2Fe-2S] Cluster

Coordinated by Cys, Glu, and His Residues. *J. Am. Chem. Soc.* **2019**, *141* (6), 2367–2375.

(24) Berkovitch, F.; Nicolet, Y.; Wan, J. T.; Jarrett, J. T.; Drennan, C. L. Crystal Structure of Biotin Synthase, an S-Adenosylmethionine-Dependent Radical Enzyme. *Science* **2004**, *303* (5654), 76–79.

(25) McLaughlin, M. I.; Lanz, N. D.; Goldman, P. J.; Lee, K.-H.; Booker, S. J.; Drennan, C. L. Crystallographic Snapshots of Sulfur Insertion by Lipoyl Synthase. *Proc. Natl. Acad. Sci. U. S. A.* **2016**, *113* (34), 9446–9450.

(26) Fuchs, M. G. G.; Meyer, F.; Ryde, U. A Combined Computational and Experimental Investigation of the [2Fe-2S] Cluster in Biotin Synthase. *J. Biol. Inorg. Chem.* **2010**, *15* (2), 203–212.

(27) Ramachandran, G.; Ramakrishnan, C.; Sasisekharan, V. Stereochemistry of Polypeptide Chain Configurations. *J. Mol. Biol.* **1963**, *7* (1), 95–99.

(28) Davis, K. M.; Schramma, K. R.; Hansen, W. A.; Bacik, J. P.; Khare, S. D.; Seyedsayamdost, M. R.; Ando, N. Structures of the Peptide-Modifying Radical SAM Enzyme SuiB Elucidate the Basis of Substrate Recognition. *Proc. Natl. Acad. Sci. U. S. A.* **2017**, *114* (39), 10420–10425.

(29) Rubio, L. M.; Rangaraj, P.; Homer, M. J.; Roberts, G. P.; Ludden, P. W. Cloning and Mutational Analysis of the Gamma Gene from *Azotobacter vinelandii* Defines a New Family of Proteins Capable of Metallocluster Binding and Protein Stabilization. *J. Biol. Chem.* **2002**, *277* (16), 14299–14305.

(30) Verghese, J.; Morano, K. A. A Lysine-Rich Region within Fungal BAG Domain-Containing Proteins Mediates a Novel Association with Ribosomes. *Eukaryot. Cell* **2012**, *11* (8), 1003–1011.

(31) Biberstine-Kinkade, K. J.; Yu, L.; Dinauer, M. C. Mutagenesis of an Arginine- and Lysine-Rich Domain in the Gp91(Phox) Subunit of the Phagocyte NADPH-Oxidase Flavocytochrome B558. *J. Biol. Chem.* **1999**, *274* (15), 10451–10457.

(32) Zhao, D.; Curatti, L.; Rubio, L. M. Evidence for NifU and NifS Participation in the Biosynthesis of the Iron-Molybdenum Cofactor of Nitrogenase. *J. Biol. Chem.* **2007**, *282* (51), 37016–37025.

(33) Jasniewski, A. J.; Wilcoxon, J.; Tanifuji, K.; Hedman, B.; Hodgson, K. O.; Britt, R. D.; Hu, Y.; Ribbe, M. W. Spectroscopic Characterization of an Eight-Iron Nitrogenase Cofactor Precursor That Lacks the “9(Th) Sulfur”. *Angew. Chem. Int. Ed Engl.* **2019**, *58* (41), 14703–14707.

(34) Jimenez-Vicente, E.; Navarro-Rodriguez, M.; Pozo-Carrion, C.; Rubio, L. M. Role of *Azotobacter vinelandii* FdxN in FeMo-Co Biosynthesis. *FEBS Lett.* **2014**, *588* (3), 512–516.



1  
2  
3  
4  
5  
6  
7  
8  
9  
10  
11  
12  
13  
14  
15  
16  
17  
18  
19  
20  
21  
22  
23  
24  
25  
26  
27  
28  
29  
30  
31  
32  
33  
34  
35  
36  
37  
38  
39  
40  
41  
42  
43  
44  
45  
46  
47  
48  
49  
50  
51  
52  
53  
54  
55  
56  
57  
58  
59  
60

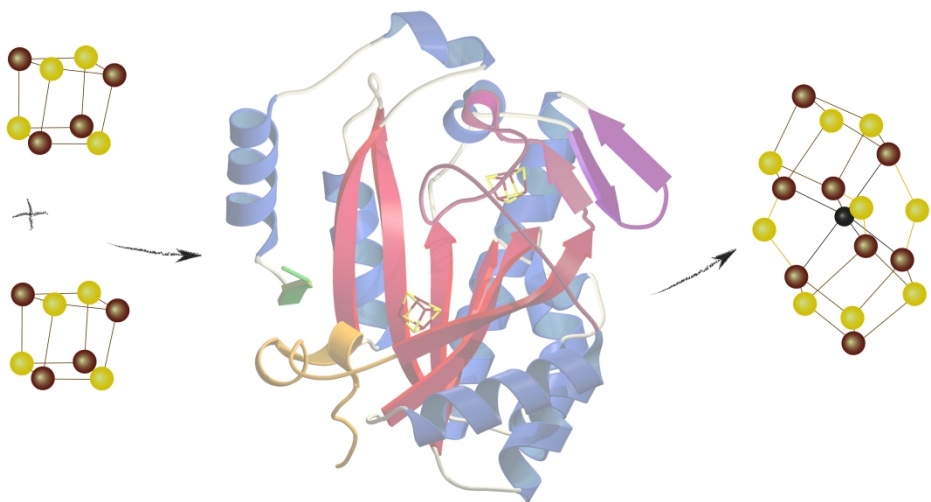
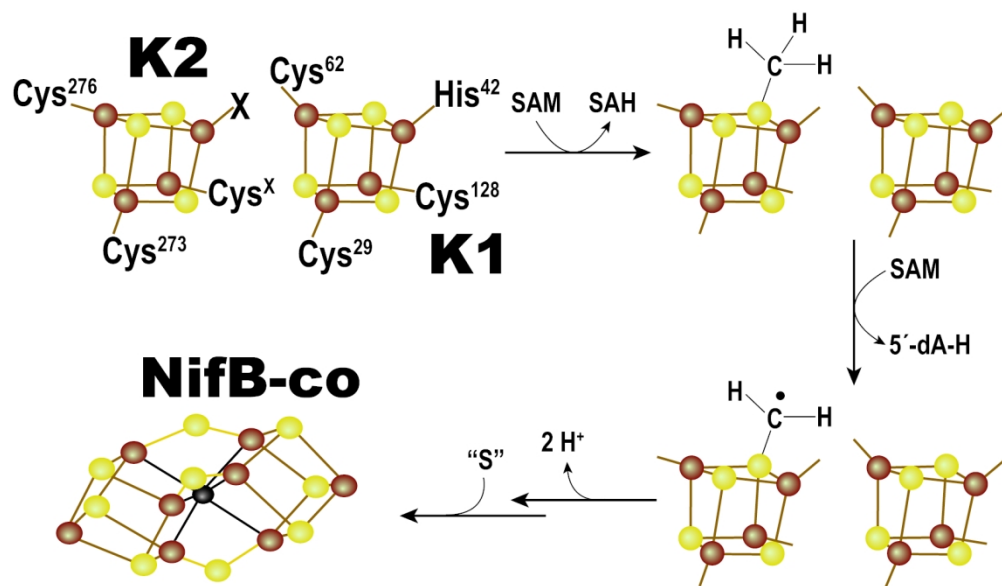


Table of content graphic artwork



Scheme 1

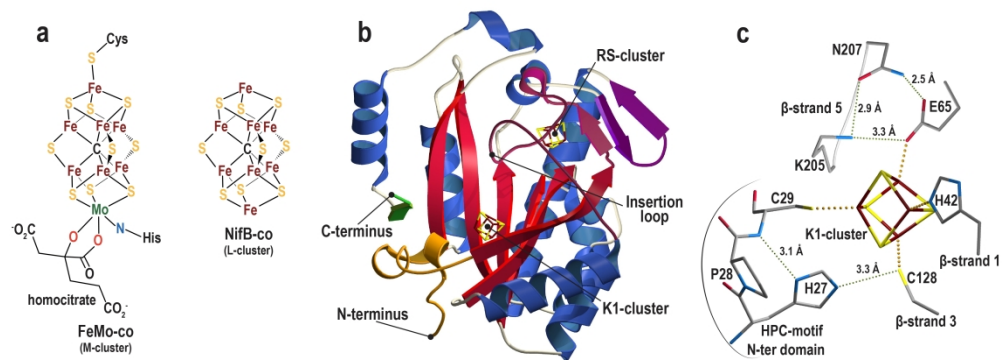


Figure 1

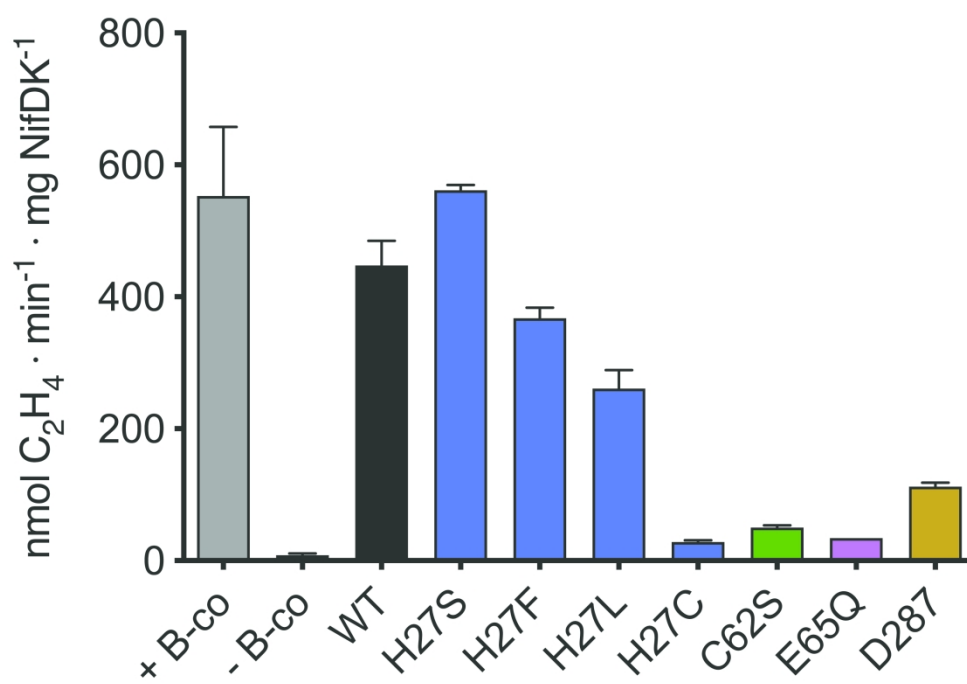


Figure 2

134x96mm (600 x 600 DPI)

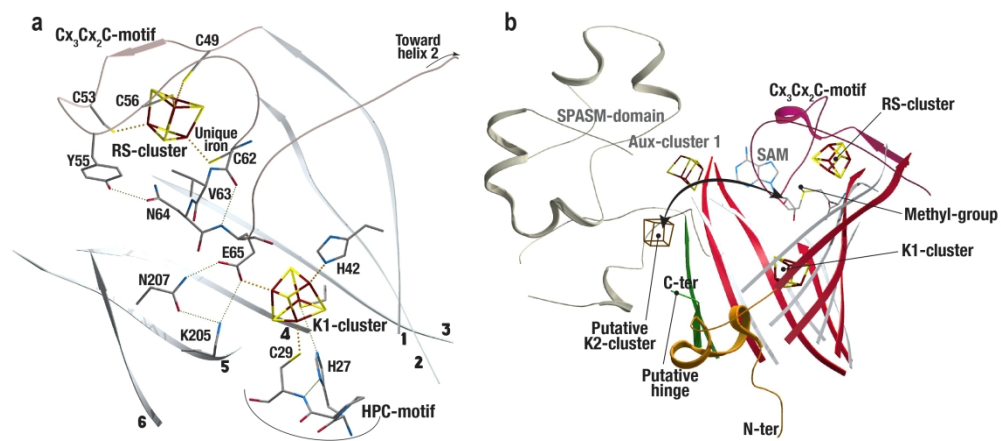


Figure 3

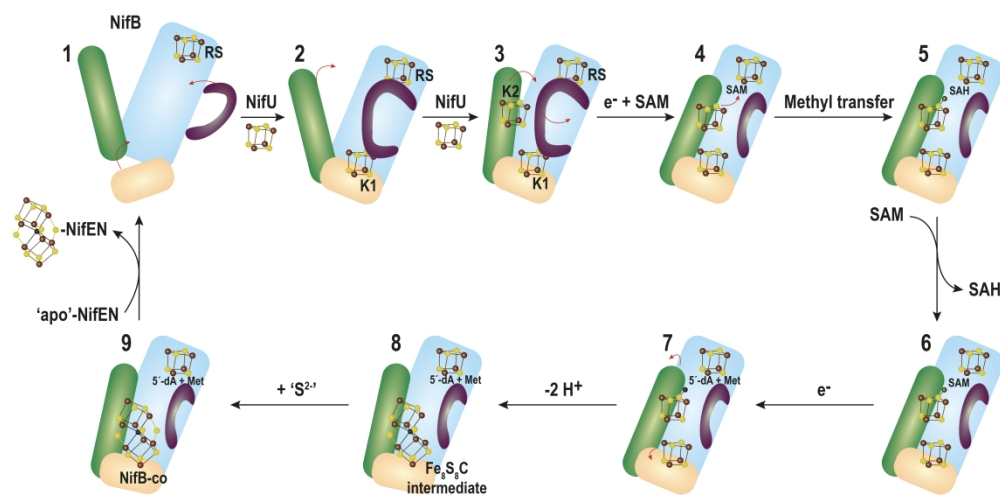


Figure 4